Supporting Information

Composition-adjustable Ag-Au Substitutional Alloy Microcages Enabling Tunable Plasmon Resonance for Ultrasensitive SERS

Xiaotian Wang,† Guanshui Ma,† Anran Li,† Jian Yu, Zhao Yang, Jie Lin, Ang Li, Xiaodong Han & Lin Guo*

Fig. S12 SERS spectra of R6G at concentration of 5×10^{-16} M absorbed on 0.35 Ag-Au SAMCs under excitation of 633 nm.

Fig. S13 SERS spectra of thiram (10^{-10} M) obtained from 0.35 Ag-Au SAMCs and Ag microcages before and after immersing into 1% H_2O_2 solution for 5 h, respectively.

Table S1. The SEM-EDX mapping analysis of the atom% of Au in the Ag-Au SAMCs via injecting different volumes of $HAuCl_4$.

Table S2. Comparing with some typical enhancement factors (EFs) of plasmonic nano/micro-structures with hollow or shape tips reported in previous literatures.

S1. Materials

In this study, copper chloride ($CuCl_2$•$2H_2O$, AR), sodium citrate (AR), acetic acid (AR), and ethanol (AR) were supplied by Beijing Chemical Works (Beijing, China), and chloroauric acid ($HAuCl_4 \cdot 4H_2O$, AR) was purchased from Aladdin Co., Ltd. (Shanghai, China). polyvinylpyrrolidone K-30 (PVP, AR), sodium hydroxide (NaOH, AR), ascorbic acid (AR), sodium borohydride ($NaBH_4$, AR), and silver nitrate ($AgNO_3$, AR) were obtained from Guangzhou Xilong Chemical Co., Ltd. (Guangzhou, China). Water was purified using a Milli-Q water system (Bedford, USA). All chemicals were used without further purification.

S2. Characterizations

The morphology of the products was investigated by field emission scanning electron microscopy (FE-SEM), for the FE-SEM measurements, a Quanta 250 FEG instrument was used, operating at an accelerating voltage of 10 KV. The transmission electron microscopy (TEM) and high-resolution transmission electron microscopy (HRTEM) analysis images as well as selected-area electron diffraction (SAED) pattern analysis were performed on a field emission transmission electron microscopy using a JEOL (TEM-2100F). The scanning transmission electron microscopy (STEM) and (energy-dispersive X-ray) EDX mapping of the porous hollow 0.35 Ag-Au alloy octahedral microcages was performed by FEI ETEM (environment transmission electron microscopy) at an accelerating voltage of 300 kV. The powder X-ray diffraction (XRD) of the samples was characterized by the Rigaku Rotaflex Dmax

2200 diffractometer with Cu Kα radiation (λ = 1.54056 Å). Absorption spectra were recorded on a UV-3600 UV-Vis-near (NIR) spectrophotometer made in Shimadzu, Japan, and solvent was ethanol. The thickness of the Ag-Au SAMCs is measured by atomic force microscopy (AFM). The microcages were cracked via a violent ultrasonic process to obtain pieces of sample for the AFM characterization. The experiment is performed by tapping mode with the tip model of OTESPA. The model of the AFM instrument is BRUKER Dimension Icon. Raman spectra were acquired with a Jobin Yvon Raman spectrometer model HR800 with the excitation wavelength of 488 nm, 514 nm, 633 nm, and 785 nm lines. The 488 nm and 514 nm are from the Ar-Kr ion laser, and the 633nm and 785nm are from the He-Ne laser. These laser power were turn to at same density around 10^9 W/m^2 (laser power: ~1.5 mW; laser spot: 1.2 μm^2) to the surface of the sample. Electrochemical measurements were carried out in a conventional three-electrode system using electrochemical analyzer (CHI 660C, CH Instruments). The as-prepared samples were used as the working electrode while a Pt plate and an Ag/AgCl/KCl (1.0 M) electrode were used as the counter and reference electrode, respectively. linear sweep voltammetry (LSV) with the potentials ranging from 10 to 150 mV (vs. Ag/AgCl) at a scan rate of 5 mV s^{-1} in a 1 M KCl solution, which has been purged by N_2 bubbling for 60 min prior to the experiment. All electrochemical experiments were performed at ambient temperature.

Table S1. The SEM-EDX mapping analysis of the atom% of Au in the 0.1~0.6 Ag-Au SAMCs via injecting different volumes of $HAuCl_4$.

Sample	0.1 Ag-Au SAMCs	0.2 Ag-Au SAMCs	0.3 Ag-Au SAMCs	0.35 Ag-Au SAMCs	0.4 Ag-Au SAMCs	0.5 Ag-Au SAMCs	0.6 Ag-Au SAMCs
Volumes of $HAuCl_4$ (mL)	0.1	0.2	0.3	0.35	0.4	0.5	0.6
Atom% of Au (SEM-EDX)	5.6%	8.1%	11.5%	14.2%	16.8%	19.3%	22.7%

Table S2. Comparing with some typical enhancement factors (EFs) of plasmonic nano/micro-structures with hollow or shape tips reported in previous literatures.

Materials	Analyte	EF	Excitation wavelength (nm)	Reference
urchin-like silver nanowire	R6G	$\sim 10^{13}$	532	[1]
Star-like gold nanoparticles	RhB	$\sim 10^{12}$	830	[2]
Ag-colloid clusters	R6G	$\sim 7\times 10^{11}$	633	[3]
Ag-Au SAMCs	**R6G**	**$\sim 1.3\times 10^{11}$**	**514**	**This work**
Au nanostars	15NAT	$\sim 10^{10}$	785	[4]
Ag nanoparticle films	CV	$\sim 10^{10}$	532	[5]
Au-Ag Alloy nanourchins	CV	$\sim 10^{9}$	633	[6]
Gold nanostars (on Au film)	4-MBA	$\sim 10^{9}$	633	[7]
Wrinkled nanoporous gold film	CV	$\sim 10^{9}$	633	[8]
Au nanoparticles with 1-nm interior gap	R6G-green	$\sim 10^{9}$	633	[9]
Nanoporous gold disk	benzenethiol	$\sim 10^{8}$	785	[10]
Mesoscopic Au meatball particles	PMA	$\sim 10^{8}$	785	[11]
p-AuAg@void@SiO_2	CV	$\sim 10^{7}$	633	[12]
Gold nanostars	4-MBA	$\sim 10^{7}$	785	[13]
Ag@Au Nanocubes	1,4-BDT	$\sim 9.7 \times 10^{5}$	785	[14]
Pd@AuCu core−shell planar tetrapods	CV	$\sim 9\times 10^{3}$	514	[15]

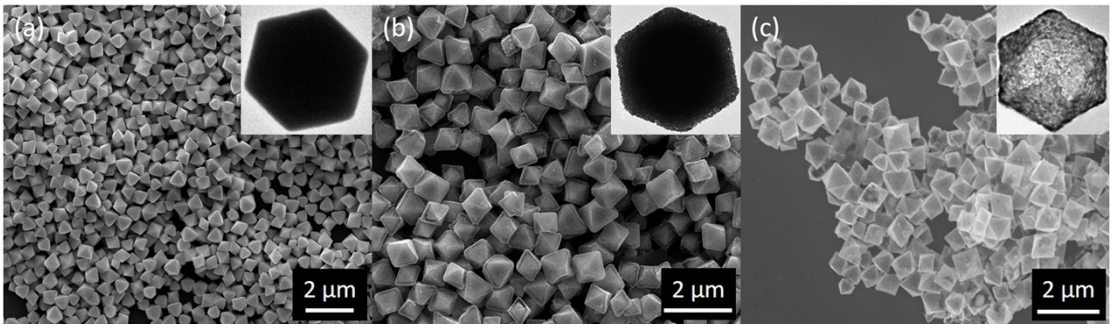

Fig. S3 SEM image and TEM image (inset) of (a) CuO_2 microcubes (b) CuO_2@Ag core-shell microstructures (c) Ag microcages.

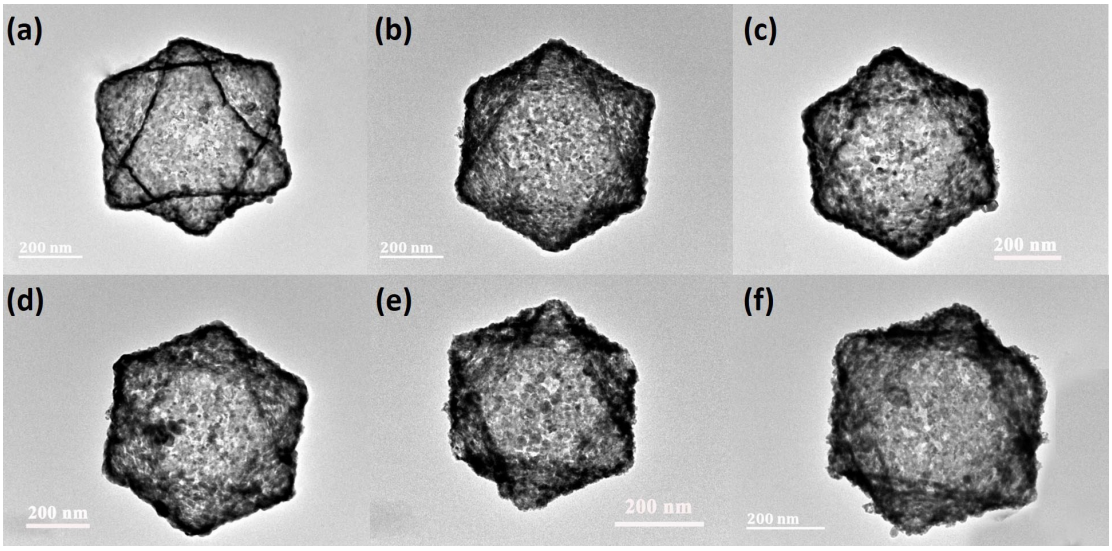

Fig. S4 Low-magnification TEM images (a)-(f) of 0.1, 0.2, 0.3, 0.4, 0.5, and 0.6 Ag-Au SAMCs.

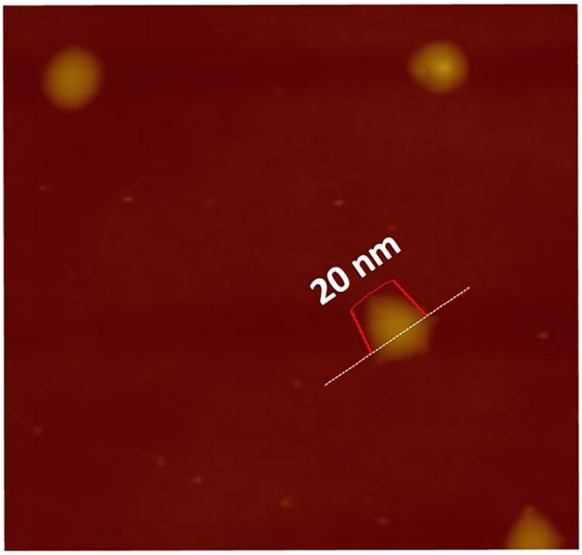

Fig. S5 AFM micrograph of the shell of 0.35 Ag-Au SAMCs.

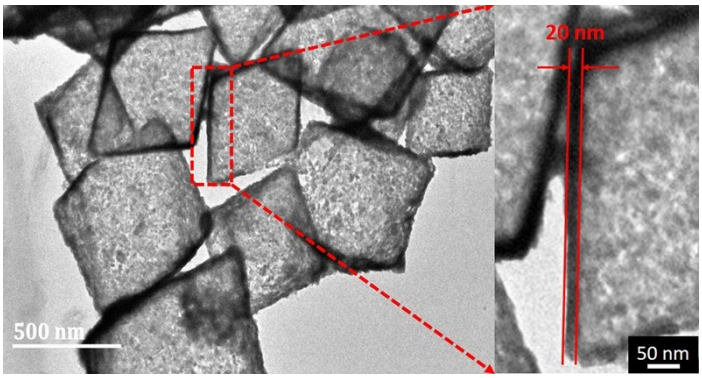

Figure S6 Thickness characterization by TEM image of 0.35 Ag-Au SAMCs.

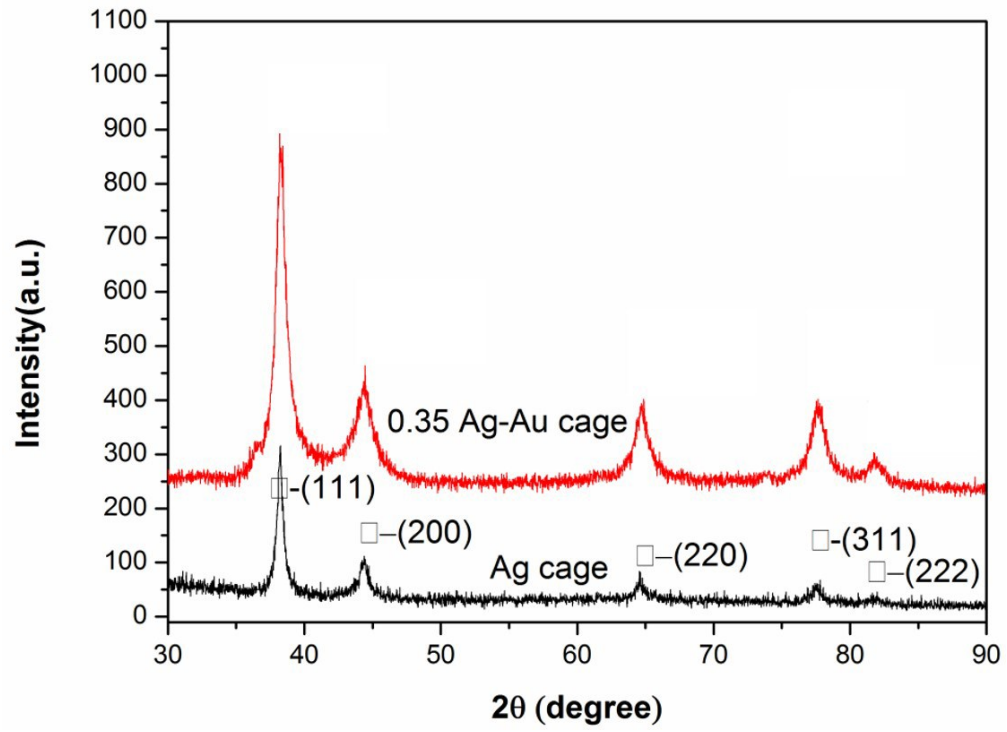

Fig. S7 XRD patterns of Ag microcages and 0.35 Ag-Au SAMCs.

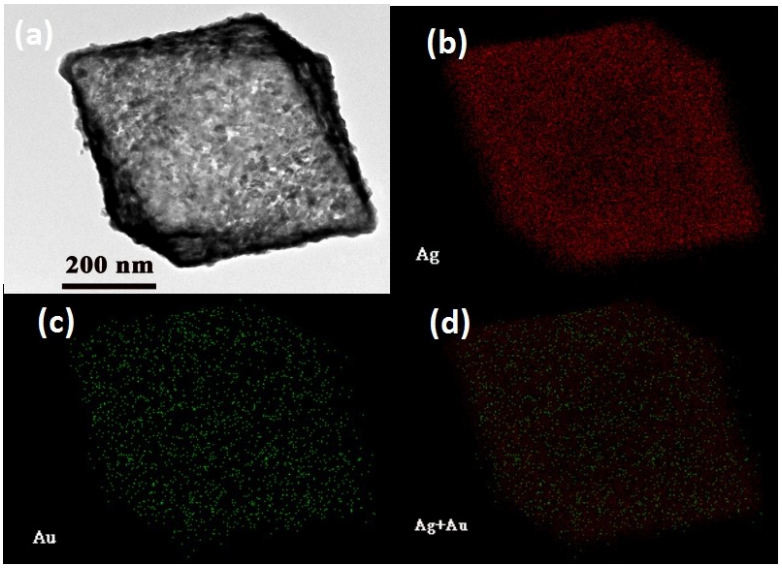

Fig. S8 (a) BF-STEM image and (b-d) EDX mapping analysis of a single 0.35 Ag-Au SAMCs.

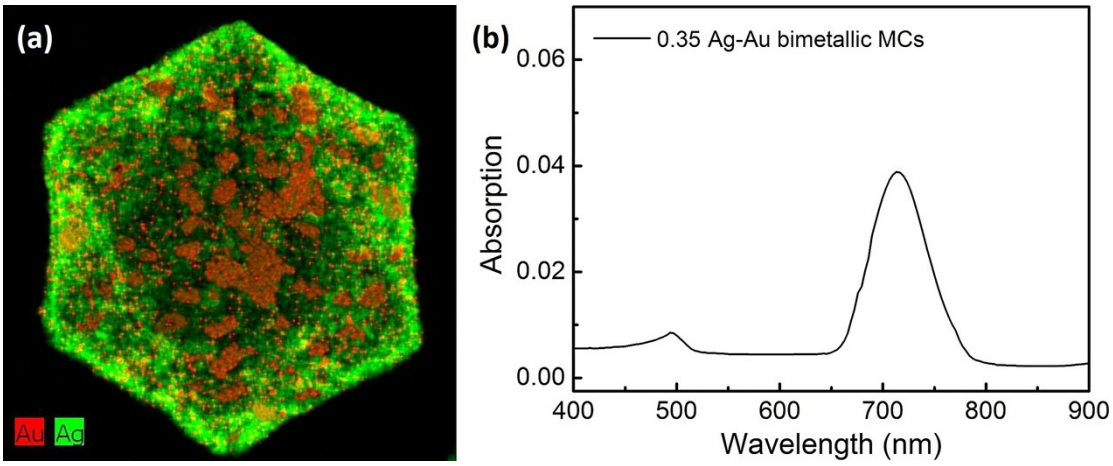

Fig. S9 (a) HAADF-STEM-EDX elemental mapping of an octahedral hollow 0.35 Ag-Au bimetallic microcage. (b) UV-vis spectra of octahedral hollow 0.35 Ag-Au bimetallic microcages as the control experiment.

S10. Finite-difference time-domain (FDTD) simulation details

The electric field distributions of the hollow and the solid octahedral MPs with 600 nm edge length are calculated using the finite-difference time-domain (FDTD) method (16). Based on the experimental results, the shell of the hollow octahedron is set to be 20 nm. For all calculations, a total-field scattered-field (TFSF) plane wave source with the wavelength of 633 nm is selected to estimate the interaction between propagating plane wave and metallic microstructures. The dielectric functions of Ag and Au were derived from the modified Drude model, considering the 8~9 Lorentzians parts (17). The dielectric function of 0.35 Ag-Au alloy was calculated based on the composition-weighted average of Au and Ag, where the Ag-Au alloy is thought to be made up of 14% Au and 86% Ag according to the value obtained by SEM-EDX mapping analysis (table S1) (18). The surrounding medium is set as vacuum. To get accurate results, an override mesh region with 3 nm mesh size enclosing the octahedral microstructure is used. Before the simulation, convergence testing was carefully done to verify the accuracy and stability of the simulations. In this research, all simulations were performed using the FDTD software (FDTD solutions 8.6, Lumerical Solutions, Inc., Vancouver, Canada).

S11. Calculation of SERS enhancement factor of the Ag-Au SAMCs

The SERS enhancement factors of R6G molecules obtained from 0.35 Ag-Au alloy microcages can be estimated by the standard equation:

$EF = (I_{SERS} / N_{ads}) / (I_{bulk} / N_{bulk})$ (1)

where N_{ads} and N_{bulk} represent the numbers of R6G (10^{-11} M) molecules absorbed on Ag-Au alloy microcages in the focus of the laser beam and the normal Raman sample, respectively. I_{SERS} and I_{bulk} are the intensities of the same vibration mode of R6G molecule obtained on Ag-Au alloy microcages and the normal Raman spectrum from solid sample, respectively.

$N_{bulk} = 6.02\times10^{23}\ mol^{-1} \times \rho \times H \times S / M = 3.6 \times 10^{11}$. (2)

where the density of R6G solid $\rho = 1.15\ g\ cm^{-3}$, molar mass (M) of R6G is 479 g/M, and Laser spot size S is about 1.2 μm^2, depth of laser penetration (H) is about 21 μm (19).

In the SERS experiment, 100 μL of an ethanol aqueous R6G solution (10^{-11} M) was dripped onto the substrate (0.4 × 0.4 cm^2), and N_{ads} can be estimated as:

$N_{ads} = 100\ \mu L \times 10^{-11}\ mol / L \times 6.02 \times 10^{23}\ mol^{-1} \times 1.2\ \mu m^2 / 0.16\ cm^2$ (3)

N_{ads} is concluded as 45. I_{SERS} and I_{bulk} are based on the R6G molecule vibration peak at 1360 cm^{-1} in SERS spectrum and normal Raman spectrum as shown in Figure S6, the intensity was obtained by take the average of 20 times measurements, I_{SERS} = 5400 and I_{bulk} = 330, also considering laser power for SERS and normal Raman. Substituting these values into the equation (1), EF of 0.35 Ag-Au alloy microcages can be calculated to be about 1.3×10^{11}. As it was assumed that 100% of the molecules are adsorbed on the sample the calculated value represents a theoretical

maximum number of adsorbed molecules, thereby the calculated EF was underestimated comparing with the actual value.

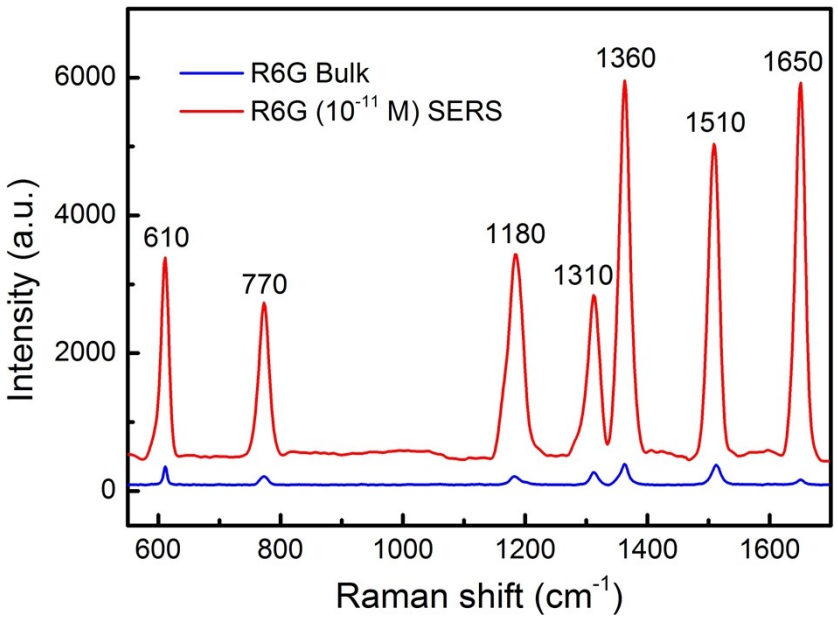

Fig. S10 Black line is normal Raman spectrum of solid R6G, red line is SERS spectrum of R6G (10^{-11} M) obtained from 0.35 Ag-Au SAMCs. Laser wavelength: 633 nm.

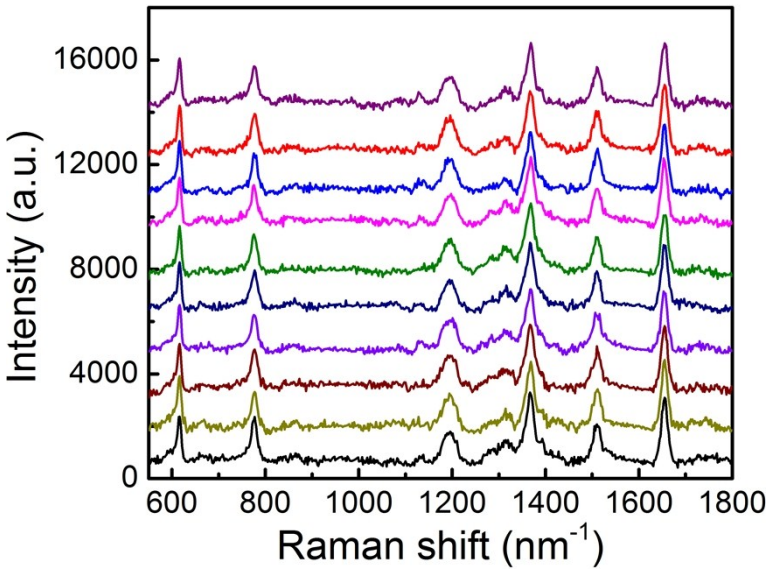

Fig. S11 SERS spectra of R6G (5×10^{-13} M) collected from ten different test spots on 0.35 Ag-Au SAMCs.

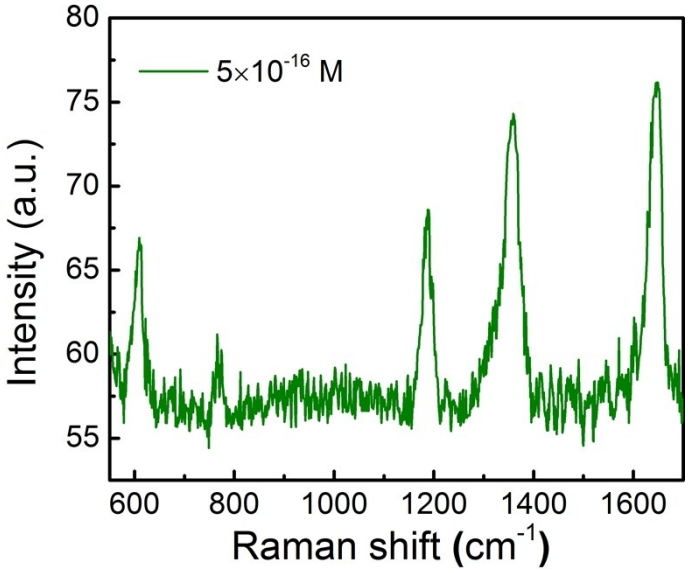

Fig. S12 SERS spectra of R6G at concentration of 5×10^{-16} M absorbed on 0.35 Ag-Au SAMCs at the excitation of 633 nm.

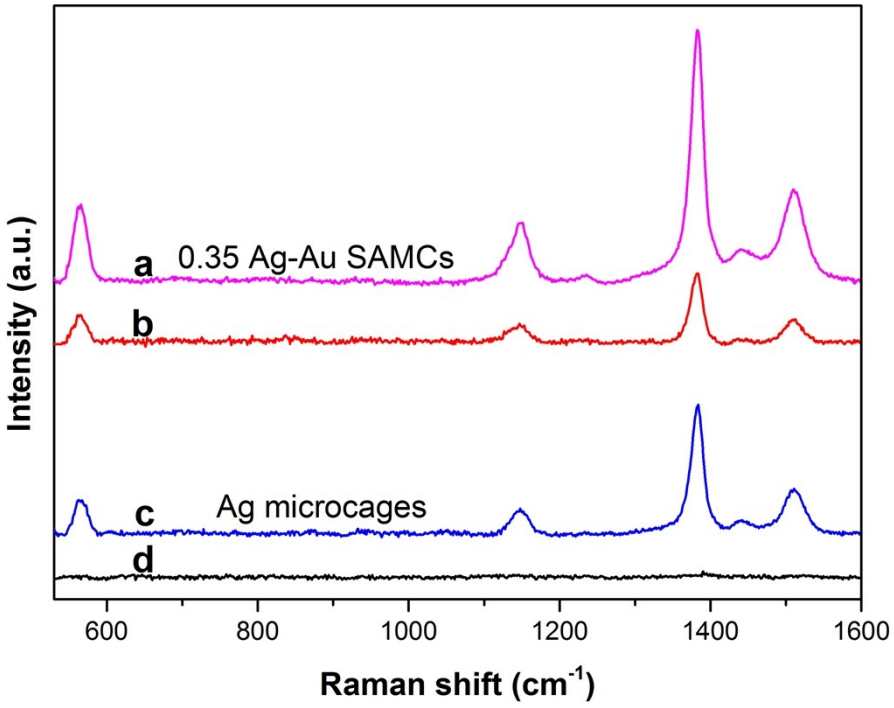

Fig. S13 SERS spectra of thiram (10^{-10} M) obtained from 0.35 Ag-Au SAMCs (a) before and (b) after immersing into 1% H_2O_2 solution for 5 h, and that of Ag microcages (c) before (d) after immersing into 1% H_2O_2 solution for 5 h.

References:

1. W. H. Hsiao, H. Y. Chen, Y. C. Yang, Y. L. Chen, C. Y. Lee, H. T. Chiu, Surface-enhanced Raman scattering imaging of a single molecule on urchin-like silver nanowires. *ACS Appl. Mater. Inter* .3, 3280 (2011).

2. L. P. Mayen, J. Oliva, A. T. Castrob, E. D. l. Rosa, SERS substrates fabricated with star-like gold nanoparticles for zeptomole detection of analytes. *Nanoscale,* 7, 10249 (2015).

3. E. C. Le Ru, E. Blackie, M. Meyer, P. G. Etchegoin, Surface Enhanced Raman Scattering Enhancement Factors: A Comprehensive Study. *J. Phys. Chem. C,* 111, 13794 (2007).

4. L. R. Lorenzo, R. A. A. Puebla, I. P. Santos, S. Mazzucco, O.Ste´phan, M. Kociak, L.M. L. Marza´n,. F. J. G. Abajo, Zeptomol Detection Through Controlled Ultrasensitive Surface-Enhanced Raman Scattering *J. Am. Chem. Soc.*131, 4616 (2009).

5. H. Y Chen, M. H. Lin, C. Y. Wang, Y. M. Chang, S. Gwo, Large-Scale Hot Spot Engineering for Quantitative SERS at the Single-Molecule Scale. *J. Am. Chem. Soc* 13, 13698 (2015).

6. Z. Liu, B. Peng, C. Cao, C.Zhang, H. You, and Q. Xiong, and J. Fang, Highly sensitive, uniform, and reproducible surface-enhanced raman spectroscopy from hollow Au-Ag alloy nanourchins. *Adv. Mater.* 26, 2431 (2014).

7. A. S. D. S. Indrasekara, S. Meyers, S. Shubeita, L. C. Feldman, T. Gustafsso,L. Fabris, Gold nanostar substrates for SERS-based chemical sensing in the femtomolar regime. *Nanoscale*, 6, 8891 (2014).

8. L. Zhang, X.Y. Lang, A. Hirata, M. W. Chen, Wrinkled nanoporous gold films with ultrahigh surface-enhanced raman scattering enhancement. *ACS Nano*, 5, 4407 (2011).

9. D. K. Lim, K. S. Jeon, J. H Hwang, H. Kim, S. Kwon, Y D. Suh J. M. Nam, Highly uniform and reproducible surface-enhanced Raman scattering from DNA-tailorable nanoparticles with 1-nm interior gap. Nature Nanotech. 6, 452 (2011).

10. J. Qi, P. Motwani, M. Gheewala, C. Brennan, J. C. Wolfe, W. C. Shih, Surface-enhanced Raman spectroscopy with monolithic nanoporous gold disk substrates. *Nanoscale*, 5, 4105 (2013).

11. H. Wang, N. J. Halas, Mesoscopic au "meatball" particles. *Adv. Mater*. 20, 820 (2008).

12. K. Liu, Y. C Bai, L. Zhang, Z. B. Yang, Q. K. Fan, H. Q. Zheng, Y. D. Yin, C. B. Gao, Porous Au-Ag nanospheres with high-density and highly accessible hotspots for sers analysis. *Nano Lett.*, 16, 3675 (2016).

13. S. Saverot, X. Geng, W. Leng, P. J. Vikesland, T. Z. Grove L. R. Bickford, Facile, tunable, and SERS-enhanced HEPES gold nanostars. *RSC Adv.* 6, 29669 (2016).

14. Y. Yang, J. Y. Liu, Z. W. Fu, D. Qin, Galvanic replacement-free deposition of Au on Ag for core-shell nanocubes with enhanced chemical stability and SERS activity. *J. Am. Chem. Soc.*136, 8153 (2014).

15. M. Meng, Z. C. Fang, C. Zhang, H. Y. Su, R. He, R. P. Zhang, H. L. Li, Z. Y. Li, X. J. Wu, C. Ma, J. Zeng, Integration of kinetic control and lattice mismatch to synthesize Pd@AuCu core-shell planar tetrapods with size-dependent optical properties. *Nano Lett.*16, 3036 (2016).

16. Taflove, A.; Hagness, S. C., Computational Electrodynamics: The Finite-Difference Time-Domain Method / Allen Taflove, Susan C. Hagness; Boston: Artech House, c2005. 3rd ed., (2005).

17. Coomar, A.; Arntsen, C.; Lopata, K. A.; Pistinner, S.; Neuhauser, D., Near-Field: A Finite-Difference Time-Dependent Method for Simulation of Electrodynamics on Small Scales. J. Chem. Phys., 135, 547 (2011).

18. Gaudry, M.; Lermé, J.; Cottancin, E.; Pellarin, M.; Vialle, J. L.; Broyer, M.; Prével, B.; Treilleux, M.; Mélinon, P., Optical Properties of (Au_{X}Ag_{1-X})_{N} Clusters Embedded in Alumina: Evolution with Size and Stoichiometry. Physical Review B, 64, 085407 (2001).

19. W. B. Cai, B. Ren, X. Q. Li, C. X. She, F. M. Liu, X. W. Cai, Z. Q. Tian, Investigation of surface-enhanced Raman scattering from platinum electrodes using a

confocal Raman microscope: dependence of surface roughening pretreatment. *Surf. Sci.* 406, 9 (1998).